AD-A181 046 GRAZING INCIDENCE X-RAY DIFFRACTION OF LEAD MONOLAYERS 1/1
AT A SILVER (111) A.. (U) PUERTO RICO UNIV RIO PIEDRAS
DEPT OF PHYSICS M G SAMANT ET AL. 12 MAY 87 TR-26
UNCLASSIFIED N00014-81-C-0776 F/G 9/1 NL

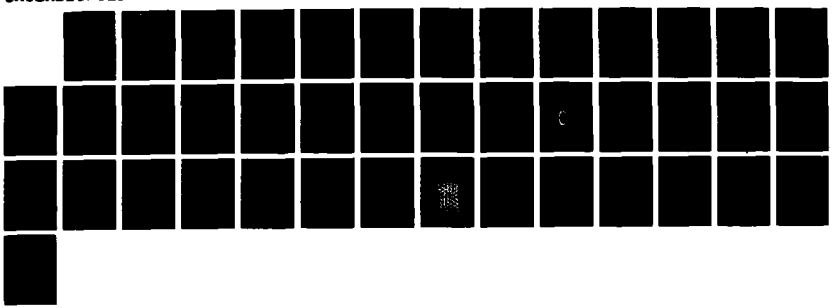

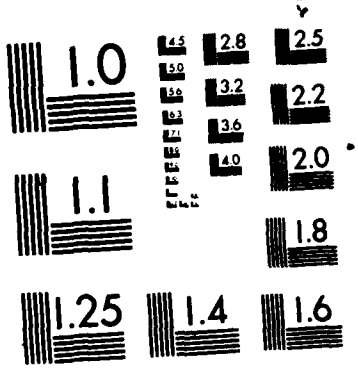

(12)

Unclassified
SECURITY CLASSIFICATION OF THIS PAGE (When Data Entered)

REPORT DOCUMENTATION PAGE		READ INSTRUCTIONS BEFORE COMPLETING FORM
1. REPORT NUMBER: Technical Report #26	2. GOVT ACCESSION NO.	3. RECIPIENT'S CATALOG NUMBER
4. TITLE (and Subtitle): Grazing Incidence X-ray Diffraction of Lead Monolayers at a Silver (111) and Gold (111) Electrode/Electrolyte Interface		5. TYPE OF REPORT & PERIOD COVERED: Interim Technical Report 6. PERFORMING ORG. REPORT NUMBER
7. AUTHOR(s): Mahesh G. Samant, Michael F. Toney, Gary L. Borges, Lesser Blum and Owen R. Melroy		8. CONTRACT OR GRANT NUMBER(s): N 00014-81-0776
9. PERFORMING ORGANIZATION NAME AND ADDRESS: Physics, Department, University of Puerto Rico Río Piedras, PR 00931		10. PROGRAM ELEMENT, PROJECT, TASK AREA & WORK UNIT NUMBERS: Task No. NR-051-775
11. CONTROLLING OFFICE NAME AND ADDRESS: Code 572-Office of Naval Research Arlington, VA 22217		12. REPORT DATE: May 12, 1987 13. NUMBER OF PAGES: 36
14. MONITORING AGENCY NAME & ADDRESS(if different from Controlling Office)		15. SECURITY CLASS. (of this report): Unclassified 15a. DECLASSIFICATION/DOWNGRADING SCHEDULE

16. DISTRIBUTION STATEMENT (of this Report)

Approved for public release, Distribution unlimited

17. DISTRIBUTION STATEMENT (of the abstract entered in Block 20, if different from Report)

18. SUPPLEMENTARY NOTES

Prepared for publication in the Journal of the American Chemical Society.

19. KEY WORDS (Continue on reverse side if necessary and identify by block number)

X-ray-electrode, interface structure.

20. ABSTRACT (Continue on reverse side if necessary and identify by block number)

Using grazing incidence geometry and a thin layer cell, x-ray scattering has been used to study the structure of electrochemically deposited monolayers of lead on silver (111) and gold (111) electrodes in-situ. For the lead monolayer deposited on silver, the lead was found to order in a hexagonal closed packed (hcp) geometry with the lead lattice compressed 1.2% relative to bulk lead. A rotational epitaxy angle of 4.4° was observed. From the width of the first order diffraction peak,

DD FORM 1 JAN 73 1473 EDITION OF 1 NOV 65 IS OBSOLETE
S/N 0102-LF-014-6601

Unclassified
SECURITY CLASSIFICATION OF THIS PAGE (When Data Entered)

cont

(300 Å)

the domain size of the lead was determined to be > Å indicating that even when deposited from a solution, the lead forms a well ordered two-dimensional solid. On a gold (111) substrate, the lead monolayer was again found to order into a hcp layer, incommensurate with the gold. The lead was compressed 0.7% relative to bulk lead, with a domain size > 200 Å.

Keywords: X-ray electrode; Lead(Metal); Gold electrode; Interface structure; Electrodeposition.

OFFICE OF NAVAL RESEARCH

CONTRACT N00014-81-C-0776

TASK No. NR 051-775

TECHNICAL REPORT #26

Grazing Incidence X-ray Diffraction of Lead Monolayers at a Silver (111) and Gold (111) Electrode/Electrolyte Interface

by

Mahesh G. Samant,* Michael F. Toney,* Gary L. Borges*, Lesser Blum** and Owen R. Melroy*

IBM Almaden Research Center, K34/802
650 Harry Road, San José, CA 95120

**Department of Physics, POB AT, Faculty of Natural Sciences, University of Puerto Rico, Río Piedras, Puerto Rico 00931

Prepared for Publication in The Journal of the American Chemical Society

Grazing Incidence X-ray Diffraction of Lead Monolayers at a Silver (111) and Gold (111) Electrode/Electrolyte Interface

Mahesh G. Samant, Michael F. Toney, Gary L. Borges, Lesser Blum[**] and Owen R. Melroy[*]

IBM Alamden Research Center, K34/802

650 Harry Road, San Jose, CA 95120

Abstract

Using grazing incidence geometry and a thin layer cell, x-ray scattering has been used to study the structure of electrochemically deposited monolayers of lead on silver (111) and gold (111) electrodes *in-situ*. For the lead monolayer deposited on silver, the lead was found to order in a hexagonal closed packed (*hcp*) geometry with the lead lattice compressed 1.2% relative to bulk lead. A rotational epitaxy angle of 4.4° was observed. From the width of the first order diffraction peak, the domain size of the lead was determined to be > 300 Å indicating that even in solution, the lead forms a well ordered two dimensional solid. On a gold (111) substrate, the lead monolayer was again found to order into a *hcp* layer, incommensurate with the gold. The lead layer was compressed 0.7% relative to bulk lead, with a domain size > 200 Å.

[**] Physics Department, College of Natural Sciences, PO. Box AT, Rio Piedras, Puerto Rico 00931

[*] To whom inquiries should be addressed.

Introduction

The structure and electronic properties of underpotentially deposited (UPD) layers on single crystal electrodes have been explored by a number of investigators.[1] Although the electronic properties have been studied *in-situ* with some success, direct determination of the atomic structure has proved elusive. This is largely because most surface techniques are based on the scattering of low energy ions or electrons. These probes are used because they have the large scattering cross sections needed for scattering at surfaces, which inherently have very few atoms. However, because of these large cross sections, they are unsuitable for use outside of vacuum. Thus, a variety of ex-situ techniques have been used[2,3] but these require transfer of the electrode from the electrochemical environment to ultrahigh vacuum (UHV). This transfer raises questions about whether the surface is the same in UHV as it was in the electrochemical environment. It has already been shown, for example, that the structure of some passive films change during transfer as hydroxyl groups decompose to oxides.[4] None the less, these ex-situ experiments have provided significant insight into the structure of atoms and molecules adsorbed from aqueous solutions onto well defined surfaces. Spectroscopic methods have also been applied to this problem (i.e., Raman,[5,6] infrared,[7-9] second harmonic generation,[10,11] reflectance,[12] and others[13,14]) but, although these can be used *in-situ*, they primarily give information on the number and orientation of adsorbed molecules, not atomic structure.

X-ray studies are particularly well suited to the electrode/electrolyte interface. Hard x-rays have a significant penetration depth in aqueous solution, and because of their wavelength they yield direct information on atomic distances and crystallographic structure. We have

previously reported surface extended x-ray absorption fine structure (SEXAFS) studies of electrochemically deposited copper monolayers on gold (111) and lead monolayers on silver (111) electrodes in contact with solution.[15,16] Grazing incidence diffraction is an equally attractive technique for probing the surface structure of electrodes and has unparalleled accuracy in determining lattice spacings and atomic positions. While EXAFS gives information on the local environment of an element, diffraction gives information on long range order. It is also far less sensitive to the Debye Waller factor than EXAFS which is an advantage when working with soft elements such as lead. Grazing incidence x-ray diffraction has already been applied to the structure determination of surface reconstruction on metals[17] and semiconductors,[18] the study of melting of adsorbed monolayers,[19] the determination of order in liquid crystal films,[20] and the characterization of solid-solid interfaces.[21] In this paper, we report the *in-situ* application of grazing incidence x-ray scattering to determine the structure of a monolayer adsorbed at a metal/solution interface. The systems chosen for this study were electrochemically deposited lead on silver (111) and gold (111) electrodes. A letter has already appeared outlining the results for the deposition of lead on silver.[22]

Experimental

Silver and Gold (111) surfaces were prepared by epitaxial evaporative deposition at 300° C onto cleaved mica substrates[23] in an Edwards E306 coater and confirmed to be (111) surfaces using Laue diffraction. Electrolytes were prepared from Aldrich ultrapure reagents with deionized water prepared from a Barnstead "nanopure" system with an "organopure" attachment. The electrolytic solution was 0.5 M sodium acetate, 0.1 M acetic acid, and 5 x 10^{-3} M lead acetate.

The electrochemical cell used and x-ray geometry are illustrated in figure 1. The cell was fabricated from Kel-f® and was approximately 3 cm in diameter and 2 cm in height. The silver and gold substrates were 1.25 cm in diameter. The electrodes (A) were held in place by small Kel-f® clamps under which electrical contact to a wire (F) was made. When placed in the cell, the silver (or gold) surface extends slightly above the outer lip of the cell allowing grazing incidence geometry to be used. The reference electrode (B) was a Ag/AgCl (3 M KCl) microelectrode, against which all potentials are reported. A Pt coil (C) was used as the counter electrode. Solutions were deoxygenated with nitrogen and added (and removed) from the cell through ports (G and H) which were sealed when not in use. The electrolyte was contained between a thin (0.5 mil) polypropylene film (D) and the electrode. This film was attached to the cell with an O-ring (E). Before the monolayer deposition, solution was added to the cell so that the polypropylene film distended somewhat, allowing the UPD layer to be deposited from bulk solution. After deposition, solution was removed, leaving only a thin layer of electrolyte between the electrode and polypropylene window. In this geometry, the diffuse x-ray scattering from the remaining liquid was of the same order as the scattering from the monolayer. For both lead on gold and silver, the UPD layer was deposited at -0.43 V. Bulk deposition occurs at -0.50 V. All experiments were conducted at room temperature.

These data were collected at the Stanford Synchrotron Radiation Laboratory (SSRL) under dedicated conditions on a focused 8-pole wiggler beam line (VII-2). A silicon (111) double crystal monochromator was used to select an incident x-ray wavelength of 1.534 Å which was calibrated by measuring the diffraction from a silicon (111) crystal. The electrochemical cell was mounted on a Huber goniometer head and attached to SSRL's four circle Huber diffractometer with the sample plane vertical during diffraction measurements. The inset in figure 1 illustrates the diffraction geometry and defines the appropriate angles. In all

experiments, the scattered beam was collected at an outgoing angle δ equal to the incident angle α. The incident beam was stopped down to a spot size of approximately 1 mm by 1 mm and its intensity monitored with a N_2 ionization chamber. The scattered radiation was collimated to 0.1 mrad. by Soller slits and collected by a scintillation detector.

Results and Discussion

The electrochemical deposition of lead on silver and gold (111) surfaces are model systems to study at the metal/liquid interface for four reasons. First, the deposition of lead on gold and silver (111) surfaces occurs in two distinct stages.[12,24-26] The first stage of electrochemical deposition occurs over a very narrow potential range and at a potential positive of the reversible Nernst potential at which bulk deposition occurs. This first stage of deposition has been termed underpotential deposition (UPD) and is believed to correspond to the deposition of a single monolayer of lead. Although no previous *in-situ* structural determination has been made, other indirect evidence strongly suggests that this layer is, in fact, a single monolayer.[12,24-27] This monolayer coverage is stable over the range of potentials (150 mV for lead on silver and 400 mV for gold) between the potential at which the "underpotential deposition" occurs and the potential for bulk deposition. The second reason this is a model system is that at full monolayer coverage, the lead forms an incommensurate layer on both gold and silver. Systems which form (1 x 1) commensurate structures are less desirable as no new diffraction peaks result from the monolayer since the in-plane d spacing is the same as the substrate's. Third, lead is a strong x-ray scatterer and offers a good chance of detecting the diffraction peaks from the monolayer. Fourth, flat (111) surfaces of silver and gold can be prepared on mica substrates. Other methods of preparing single crystal surfaces often results in rough or waffled surfaces which are unsuitable for grazing incidence diffraction. Grazing

incidence geometry is used because the small penetration depth of the x-rays into the substrate results in very little diffuse substrate scattering and because of the electric field is enhanced at the surface.[28]

Just as in normal 3-dimensional diffraction, surface diffraction peaks result from satisfying the Bragg condition in the overlayer;

$$n\lambda = 2d \sin(\theta) \qquad (1)$$

where λ is the wavelength of the incident light, d is the spacing between diffracting rows, θ is the Bragg angle and n is an integer. Because the diffraction is two dimensional, the d spacing is now the spacing between rows instead of planes as in 3-dimensional diffraction. Another difference between 2 dimensional and 3 dimensional diffraction is that the Bragg points in 3 dimensional diffraction become Bragg rods in 2 dimensional. These rods are perpendicular to the surface and the intensity along the rod is constant.

Two reflections for a hexagonal closed packed (*hcp*) layer are schematically illustrated in figure 2. The (10) reflection has the largest d spacing and hence will be the strongest reflection. For this geometry, the nearest neighbor distance can be easily calculated from the d spacing measured from either of the reflections. On further inspection, it is clear that each of these reflections will have six fold symmetry. The (10) and (11) reflections (having six fold symmetry) are unique to hexagonal structures and their observation from a surface layer proves that the structure is a 2 dimensional hexagonal array.

The notation used above, which will be used throughout the manuscript, applies to a 2-dimensional layer but is also used extensively to describe the substrate in LEED. The

relationship between this 2 dimensional notation and the conventional 3-dimensional (hkl) notation for a fcc crystal is as follows:

$(10) = \frac{1}{3}(\bar{4}22)$

$(11) = (\bar{2}02)$

It should be noted that for a (111) fcc surface the $\frac{1}{3}(\bar{4}22)$ is a crystal truncation rod not a surface diffraction peak as will be discussed below.

Silver Diffraction

The truncation of a crystal at its surface results in the creation of a significant amount of scattering intensity far away from the Bragg points which is spread right across the Brillouin zone. Measurements of this scattering have recently been reported by Robinson[29] and were shown to be sensitive to the crystal perfection and to surface roughness. These streaks of intensity have been termed Crystal Truncation Rods (CTR).[29] For a (111) fcc surface, the $\frac{1}{3}(\bar{4}22)$ reflections are in fact CTR's. The scan of the CTR of the silver (111) electrode immersed in solution is shown in figure 3a. Changing the incidence angle α ($\alpha = \delta$) corresponds to changing the perpendicular momentum transfer. The angle at which the small peak occurs is the critical angle for the air/water/silver interface and is 0.60° in this experiment. A rocking scan of this CTR taken at the critical angle is shown in figure 3b. Rocking scans correspond to holding the scattering angle (2θ) and the Bragg angle (θ) fixed and rotating the sample about the azimuthal angle, ϕ. This peak is approximately 0.2° broad which indicates a fairly well ordered, smooth surface. The radial scan of the CTR is shown in figure 3c. Radial scans are scans of θ and 2θ at a fixed azimuthal angle. These scans represent the first reported observation of CTR's at a solid/solution interface and indicate that

in future experiments, it may be possible to observe roughening of single crystal electrodes in solution using this technique. The azimuthal angle at which the CTR occurred in the rocking scan was defined to be $\phi = 0^\circ$ and is used as a reference for other reflections.

The CTR of a (111) surface has 6 fold symmetry and indeed, identical reflections were observed at 60° intervals. The silver lattice parameter calculated from these scans is 4.08 Å, in agreement with the known nearest neighbor distance for silver. It is important to measure the CTR's of the substrate not just for characterization but also because its intensity is of the same order as that from a single layer of adsorbed atoms.[29] If the substrates are not of high enough quality to allow observation of the CTR's, it is unlikely that the diffraction from ordered adsorbed monolayers will be measurable.

Lead on Silver (111)

Analogous scans to that shown for the silver CTR are shown for the (10) reflection from a monolayer of lead deposited on the silver (111) surface in figures 4a-c. The electrode potential was -0.43 V, at which the monolayer is at full coverage. The rocking scan taken at 0 V, a potential at which the lead is oxidized and dissolves into solution, is shown in figure 5. The disappearance of the diffraction peak shows that the peak in figure 4b does, in fact, result from the lead monolayer. Like the silver CTR, the peak in the Bragg rod for lead on silver (111) occurs at the critical angle, 0.54°. This is 0.06° less than that observed for the silver CTR and may reflect a slight change in the roughness of the surface. Under potential control, thin silver films on mica are known to become smoother.[30] This angle is used in all other measurements of the lead scattering. Again, the large diffuse scattering background is a result of the thin layer of solution covering the electrode. There are two important features in figure 4b. First,

the position of the diffraction peak is rotated 4.4° from the direction of the silver CTR, which by initial assignment, occurs at 0°. Second, the width of the lead reflection (approximately 0.2°) is comparable to the width observed for the silver CTR in figure 2. This clearly means that even in solution, the lead monolayer forms a well ordered two dimensional solid. The rotational epitaxy angle of 4.4° is almost identical to that reported by Takayanagi et al.[12] and Rawlings et al.,[31] who studied the vapor deposition of lead on silver (111) in UHV with LEED. As in the rocking scan, the radial scan in figure 4c has a similar width to that of the radial scan of the silver CTR. The FWHM of this peak in radians ($\Delta\theta$) is related to the domain size of the lead crystallites (L) by the Scherrer formula:

$$L = 0.9 \frac{\lambda}{\Delta\theta \cos\theta} \qquad (2)$$

Where λ is the x-ray wavelength, and θ is the Bragg angle. From figure 4, this domain size is calculated to be > 300 Å. Similar values are obtained using the width of the other diffraction peaks. The domain size is reported as a lower limit since the instrumental broadening has not been deconvoluted. This is probably not an inherent limit to the domain size but rather limited by the defects in the silver crystal. It is, however, comparable to that observed for a vapor deposited lead monolayer on copper (110).[32]

In addition to the lead reflection observed at $\phi = +4.4°$, there is a similar reflection observed at $\phi = -4.4°$. Both reflections are shown in figure 6a (a linear background was subtracted from the data). This plus/minus symmetry with respect to the underlying surface results from different domains of lead. There is no energetic difference between the lead orientating +4.4° or -4.4° relative to the silver and any given domain has an equal chance of possessing each alignment. Although the intensities of the two peaks are different, it must be mentioned

that a fresh monolayer was deposited between each scan. There is, however, precedence for differences in the intensities of these peaks. For example, large differences in the diffraction intensities from different domains have been observed for O_2 and D_2 on graphite using LEED.[33] The (11) and (20) reflections from the lead monolayer are also observed although the (20) reflection is very weak because of the large Debye Waller factor. The (11) reflection is shown in figure 6b. Like the (10) reflection, there are two peaks separated by 8.8°, but now centered with respect to the direction of the silver ($\bar{2}02$) reflection.

As expected for a hexagonal array of lead atoms, similar reflections are observed at 60° intervals (six fold symmetry). From the scattering angles of the reflections, and using equation 1, the lead nearest neighbor distance is found to be 3.459 Å ±0.002. Identical distances are obtained from each reflection. This is a 1.2% contraction from the nearest neighbor distance in bulk lead (3.501 Å). From this nearest neighbor distance and the six fold symmetry of the observed reflections, the monolayer of lead can unambiguously be shown to be a ***hcp*** layer. The structure of the lead monolayer and underlying silver is shown in figure 7a. The open circles represent the underlying silver atoms and the shaded circles, the atoms in the lead overlayer, which is incommensurate (the lead lattice is not simply related to the silver lattice). The rotational epitaxy angle of 4.4° is shown. This structure is in excellent agreement with that predicted from electrochemical data where, assuming that two electrons are transferred in the deposition of each Pb^{2+} atom, the charge measured for the UPD is consistent with the formation of a closed packed monolayer of lead atoms. The electrochemical experiments are not sensitive enough to measure the 1.2% contraction and, of course, contain no information on the rotational epitaxy angle.

A construction of the expected LEED pattern for this structure is shown in figure 7b. LEED spots from silver are denoted by open circles and those from lead by closed circles. The center of the pattern is marked by a "+". Only the (10) and (11) reflections from lead and the $\frac{1}{3}(\bar{4}22)$ and the $(\bar{2}02)$ silver reflections are shown. Since most structural work on monolayers at electrode surfaces has been performed ex-situ with LEED, this is perhaps a more familiar form of presentation. It is easy to understand the x-ray diffraction results in terms of this diagram. The rod scans in the diffraction experiment are scans perpendicular to the palne of the paper. Rocking scans correspond to looking at a fixed radius from the center of the LEED pattern and varying the angle. The radial scans then correspond to a fixed angle with a varying radius. This also illustrates why the silver diffraction peak is not observed in the rocking scans shown in figure 6.

As mentioned earlier, this pattern has essentially been observed for vapor deposited lead on silver (111).[12,31] The contraction of the lead lattice was observed in the LEED experiment was less than that observed here, but the resolution of LEED is insufficient to resolve this small difference. This strongly suggests that for this system, even though the two environments are very different, the deposition of lead at the vacuum/silver (111) interface is very similar to the electrochemical deposition of lead on silver (111). The 1.2% contraction is probably caused by the lead-silver bonds being stronger than the lead-lead bonds, which is reflected in the 0.3 eV excess adsorption energy. For an incommensurate layer, this makes it energetically more favorable to pack more lead atoms on a silver (111) surface than on a lead surface. One must also note that in the monolayer, the lead-lead bond strength may be different from bulk lead since the lead is an adsorbed monolayer and in contact with solution.

The structure presented in figure 7a is close to a ($\sqrt{28}$ x$\sqrt{28}$) R40.9° superlattice, and in fact, this structure has been proposed for vapor deposited lead on gold (111).[34] The nearest neighbor distance in this structure would be 3.50Å. This distance is larger than that observed by 1.2% and so the $\sqrt{28}$ x$\sqrt{28}$ structure can be ruled out. The close proximity of this 'higher order' superlattice may, however affect the rotation epitaxy angle. McTague and Novaco have developed a model for predicting the strain energy of an incommensurate overlayer as a function of its orientation with respect to the substrate. The rotational epitaxy angle is then the angle at which this strain energy is minimized. Using this model, a rotational epitaxy angle of 6.5° is predicted for the incommensurate layer of lead on silver (111). These predictions are frequently within a few tenths of a degree from that measured,[35] so the 2.1° deviation measured here is significant. Although the cause for this deviation is unclear, there are two likely possibilities. First, in the McTague Novaco model, the overlayer is approximated as a harmonic solid and this is probably inadequate for lead, since the melting temperature is low and thermal motion is large at room temperature. Second, the existence of superlatticies can affect this angle and it seems probable that the nearness of the $\sqrt{28}$ x28 superlattice has a strong influence on the rotational epitaxy angle. This has been proposed to explain the discrepancy between the model and experiment for Ne physisorbed on the basal plane of graphite.[36]

Lead on Gold (111)

Measurements of the CTR of the gold (111)/air interface are shown in figures 8a-c. The gold substrates are of lower quality than the silver. The rocking scans of the gold CTR are much broader than those for silver, while the radial scans are of similar width. Correspondingly, the signal to noise is lower. This increased breadth is a manifestation of a spread in the alignment

of the gold (111) crystallites on the mica (mosaic spread). This is not, however, reflected in the electrochemistry of this surface. The UPD of lead on this surface results in a classic cyclic voltammogram for deposition on gold (111).

Even with this lack of perfect registry of the gold crystallites with the mica substrate, the substrates are good enough too allow observation of the diffraction peaks from the monolayer of lead. These scans are shown in figure 9a-b. With the mosaic spread in the gold surface, the rocking scan is so broad that one can not determine the rotation epitaxy angle (or if in fact there are two peaks), although it is between 0° and 8°. The lead-lead lattice spacing measured from the radial scans is 3.476 ± 0.003 Å, a 0.7% contraction from bulk lead. From the width of the peak in the radial scan, the domain size is estimated to be > 200 Å. This is consistent with the estimated domain size of the gold substrate.

The (11) lead reflections were also observed although they were weaker than the (10) diffraction peaks. The (20) reflections could not be distinguished from the background. As expected, the (10) and (11) reflections were observed to have 6 fold symmetry. This, coupled with the lead-lead spacing, proves that the monolayer of lead is a *hcp* layer. As observed for lead deposition on silver, the lead-lead distance is inconsistent with the $\sqrt{28}$ x$\sqrt{28}$ higher order superlattice structure which was proposed for vapor deposited lead on gold.[34] The similarity between the electrochemical and vapor deposition of lead on gold and silver suggests that this structure may not exist in vapor deposited lead on gold either. The bond distances measured in this experiment are sufficiently close to that which would exist in the $\sqrt{28}$ x$\sqrt{28}$ structure that LEED would not be able to distinguish between them.

For lead on gold, the McTague Novaco model predicts a rotational epitaxy angle of 6.8° Even with the poor quality of the rocking scans, this angle would seem to be larger than that observed. This prediction is also inconsistent with that observed for vapor deposited lead on gold (4.3°).[34] Again, like lead on silver, the closeness of the superlattice structure may be the cause of this deviation.

Conclusions

This work demonstrates that *in-situ* structural determination at the metal/solution interface is possible using grazing incidence x-ray diffraction. Underpotential deposition of lead on silver (111) was found to form a *hcp* layer 1.2% compressed relative to bulk lead. This layer is incommensurate with the silver substrate, and the lead crystal lattice is orientated relative to the silver lattice with a 4.4° rotational epitaxy angle. The underpotential deposition of lead on gold (111), at full monolayer coverage, was found to produce a *hcp* layer compressed 0.7% relative to bulk lead. Due to the mosaic nature of the gold substrate, the rotational epitaxy angle could not be determined. Further work is in progress to improve the gold substrates so that these measurements can be made for this and other systems.

The ability to perform structural analysis at the metal/solution interface *in-situ* should not only help advance our knowledge of this important interface but also act as a bridge between ex-situ measurements and the interface as it exists in solution.

Acknowledgements

This work was partially supported by the Office of Naval Research and was carried out at the Stanford Synchrotron Radiation Laboratory (SSRL) which is supported by the Department of Energy. We wish to thank Joseph G. Gordon II for many useful discussions and Sean Brennan for his help with the experimental apparatus at SSRL. Without the help of these individuals and institutions, this work would not have been possible.

References

1. see for example: D. Kolb in *Advances in Electrochemistry* H. Gerischer and C. Tobias, Eds., Vol II, Wiley: New York, 1978, p 125.

2. A. Hubbard, Acc. Chem. Res., *13*, 177 (1980).

3. P. Ross, Surface Science, *102* 463 (1981).

4. R. Hoffman, in *Passivity in Metals and Semiconductors*, M. Froment Ed., Elsevier: Amsterdam, 1983, p.147.

5. R. Chang and T. Furtak, *Surface Enhanced Raman Scattering*, Plenum Press, New York, 1982.

6. M. Weaver, F. Barz, J. Gordon and M. Philpott, Surface Science, *125*, 409 (1983).

7. S. Pons, J. Electroanal. Chem., *150*, 495 (1983).

8. A. Bewick, J. Electroanal. Chem., *150*, 481 (1983).

9. K. Kinimatsu, H. Seki, W. Golden, J. Gordon and M. Philpott, Langmuir, *2*, 464 (1986).

10. R. Corn, M. Romagnoli, M. Levenson and M. Philpott, J. Chem. Phys., *81*, 4127 (1984)

11. G. Richmond, Langmuir, *2*, 132 (1986).

12. K. Takayanagi, D. Kolb, K. Kambe and G. Lehmpfuhl, Surface Science, *100*, 407 (1980).

13. R. Muller and J. Farmer, Surface Science, *135*, 521 (1983).

14. J. Gordon and S. Ernst, Surface Science, *101*, 499 (1980).

15. L. Blum, H. Abruna, J. White, J. Gordon, G. Borges, M. Samant and O. Melroy, J. Chem. Phys., *85*, 6732 (1986).

16. M. Samant, G. Borges, J. Gordon, L. Blum and O. Melroy, J. Am. Chem. Soc., (in press).

17. I. Robinson, Phys. Rev. Lett. *50*, 1145 (1983).

18. J. Bohr, R. Feidenhans'l, M. Nielsen, M. Toney, R. Johnson, and I. Robinson, Phys Rev Lett. *54*, 1275 (1985).

19 W. Marra, P. Fuoss, and P. Eisenberger, Phys. Rev Let., *49*, 1169 (1982).

20. D. Moncton and R. Pindak, Phys. Rev. Lett. *43*, 701 (1979).

21. W. Marra, P. Eisenberger, and A. Cho, J. Appl. Phys. *50*, 6927 (1979)

22. M. Samant, M. Toney, G. Borges, L. Blum, and O. Melroy, Phys. Rev. Lett., (in press).

23. K. Reichelt and H. O. Lutz, J. Cryst. Grow., *10*, 103 (1971).

24. A. Hamelin, J. Electroanal. Chem. *165*, 167 (1984).

25. A. Hamelin, J. Electroanal. Chem. *101*, 285 (1979).

26. J. Schultz and D. Dickertmann, Surf. Sci., *54*, 489, (1976).

27. O. Melroy, K. Kanazawa, J. Gordon, and D. Buttry, Langmuir, *2*, 697 (1986).

28. G. Vineyard, Phys. Rev. B, *26*, 41 (1982).

29. I. Robinson, Phys. Rev. B, *33 (6)*, 3830 (1986).

30. R. Waser and K. Weil, J. Electroanal. Chem., *150*, 89 (1983).

31 K. Rawlings, M. Gibson and P. Dobson, J. Phys. D: Appl. Phys *11*,2059 (1978).

32. S. Brennan, P. H. Fuoss, and P. Eisenberger, Phys. Rev. B, *33* (6), 3678 (1986).

33. M. Toney and S. Fain, (Submitted Phys. Rev. B); J. Chui and S. Fain, private communication.

34. J. Perdereau, J. Biberian, and G. Rhead, J. Phys. *F4*, 798 (1974).

35. C. Shaw, S. Fain, and M. Chinn, Phys. Rev. Lett.,*41*, 955 (1978).

36. L. Bruch, Surface Sci. *115*, 167 (1982).

Figure Captions

Figure 1. Electrochemical Cell: A) Silver or Gold (111) electrode, B) Ag/AgCl reference electrode, C) Platinum counter electrode, D) Polypropylene window, E) O-ring holding polypropylene to cell, F) External electrical connection to the working electrode, G) Solution inlet, and H) Solution outlet.

Insert: Grazing incidence scattering geometry showing the incident angle α, the output angle δ, the scattering angle θ, and the azimuthal angle ϕ. In all experiments reported here, $\alpha = \delta$. I_0 is the incident beam, I_s the scattered beam which goes to the Soller slits and detector, and I_r is the specular reflection.

Figure 2. Reflections from a 2-dimensional hexagonal layer. a) The (10) reflection. b) The (11) reflection.

Figure 3. Crystal truncation rod for a silver (111)/solution interface. a) Crystal truncation rod scan at $2\theta = 35.848^\circ$ and $\phi = 0^\circ$ b) Rocking scan at $2\theta = 35.848^\circ$ and $\alpha = \delta = 0.60^\circ$. c) Radial scan at $\phi = 0^\circ$ and $\alpha = \delta = 0.60^\circ$.

Figure 4. (10) reflection of the lead monolayer on silver (111). a) Bragg rod scan at $2\theta = 29.688^\circ$ and $\phi = 4.4^\circ$. b) Rocking scan at $2\theta = 29.688^\circ$ and $\alpha = \delta = 0.54^\circ$ c) Radial scan at $\alpha = \delta = 0.54^\circ$ and $\phi = 4.4^\circ$

Figure 5. Rocking scan of the silver (111) surface at 0 V. All other parameters as in 4b.

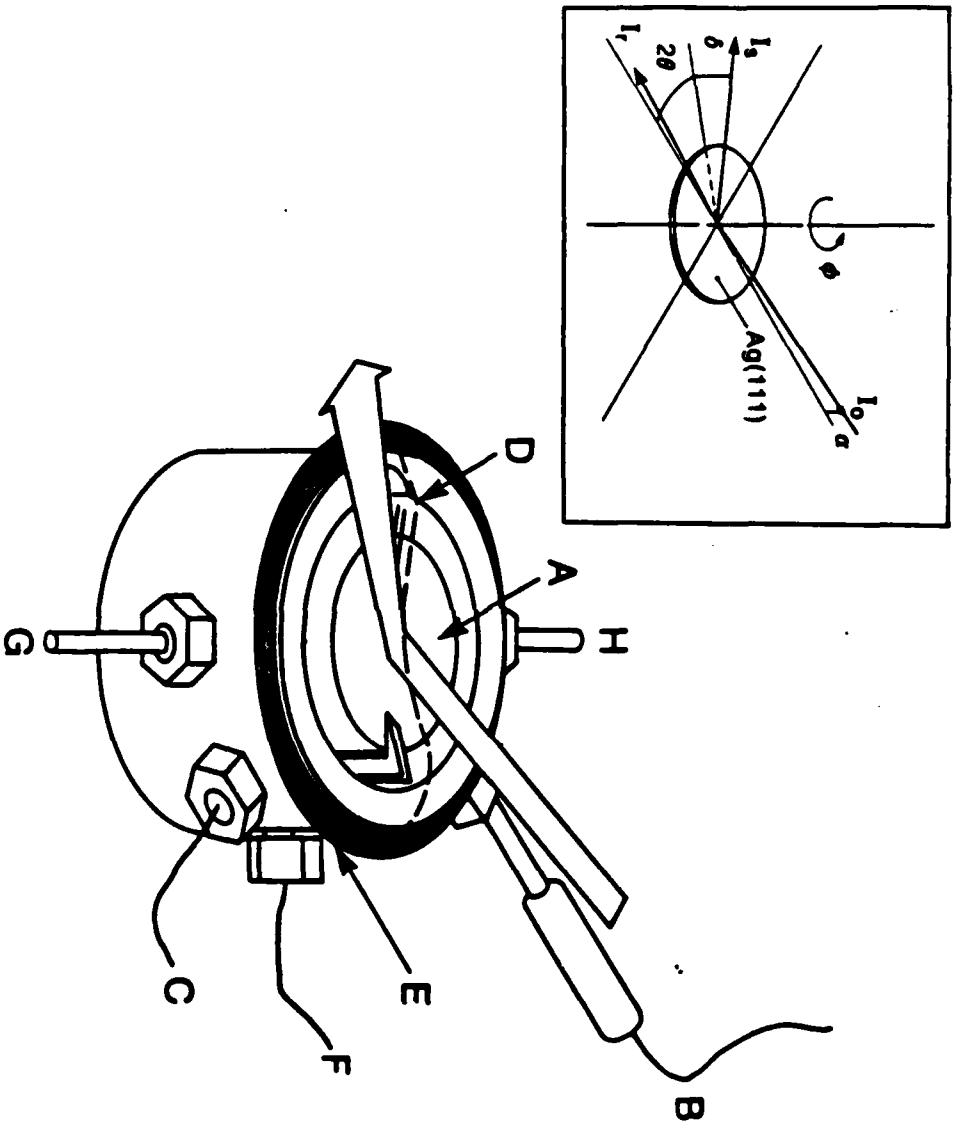

Fig 1

(10) Reflection Rows

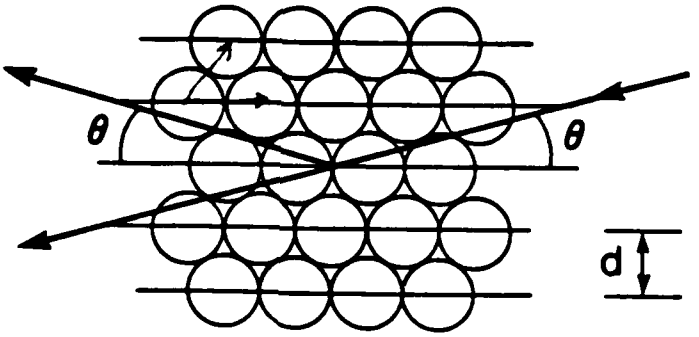

Fig 2a

(11) Reflection Rows

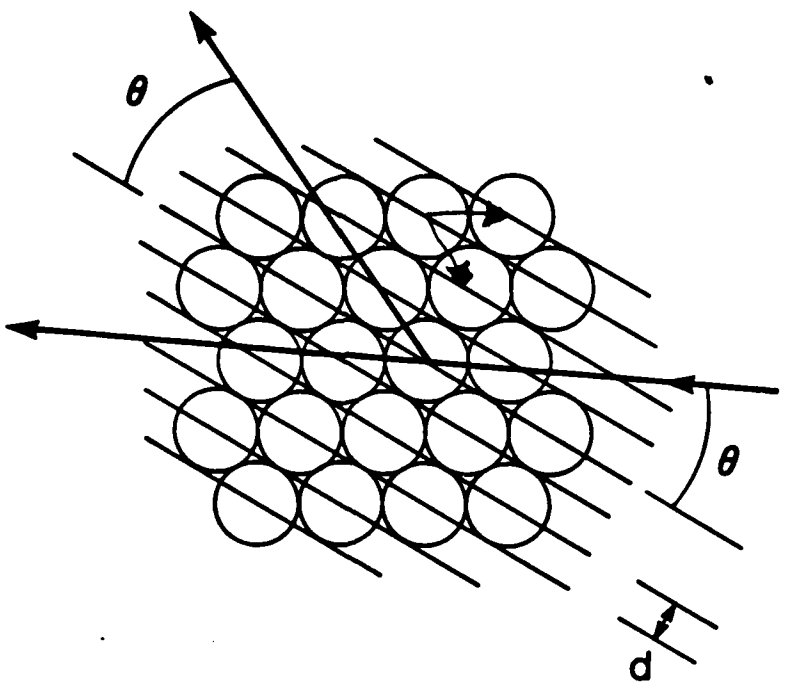

Fig 26

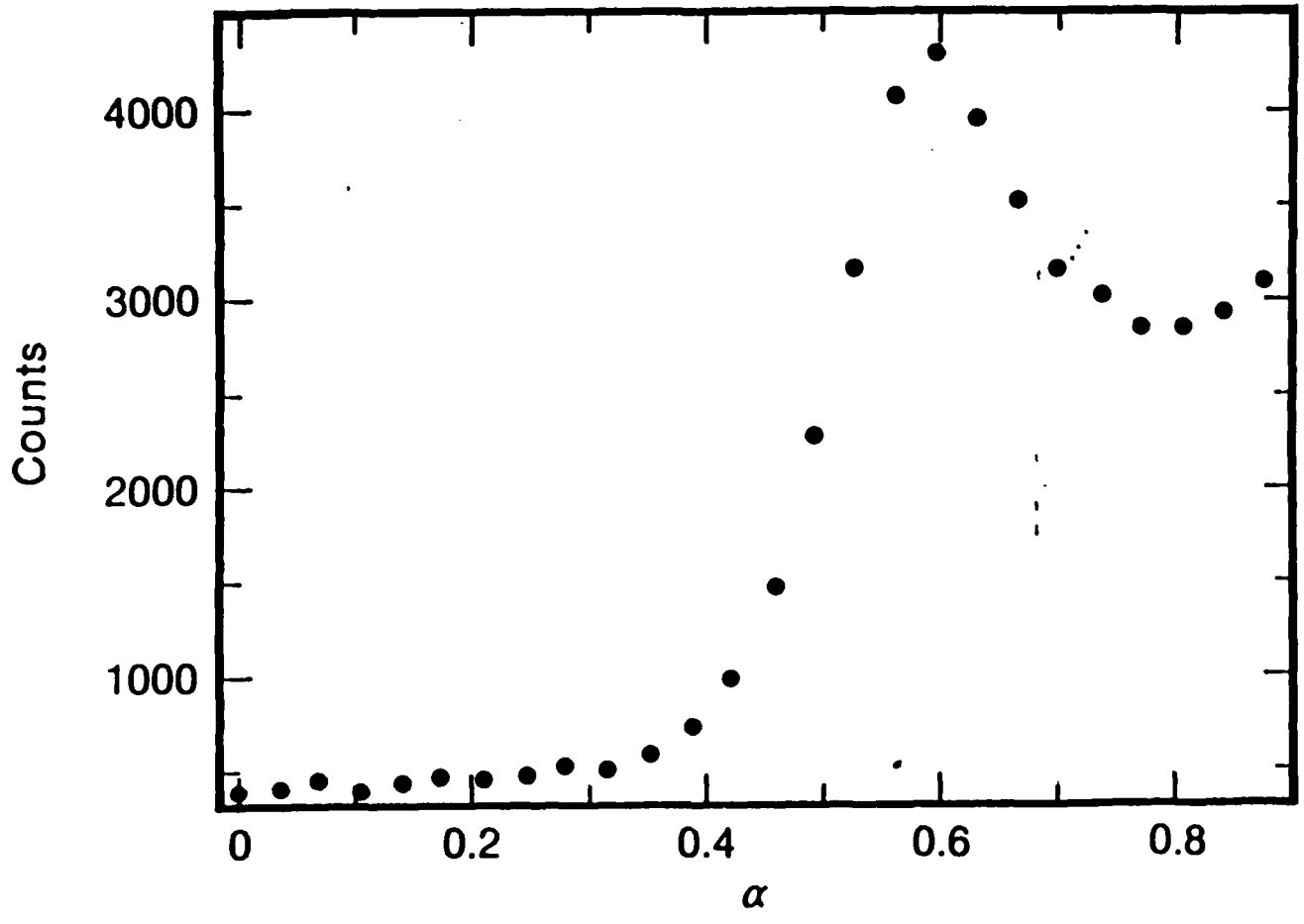

Fig 3c

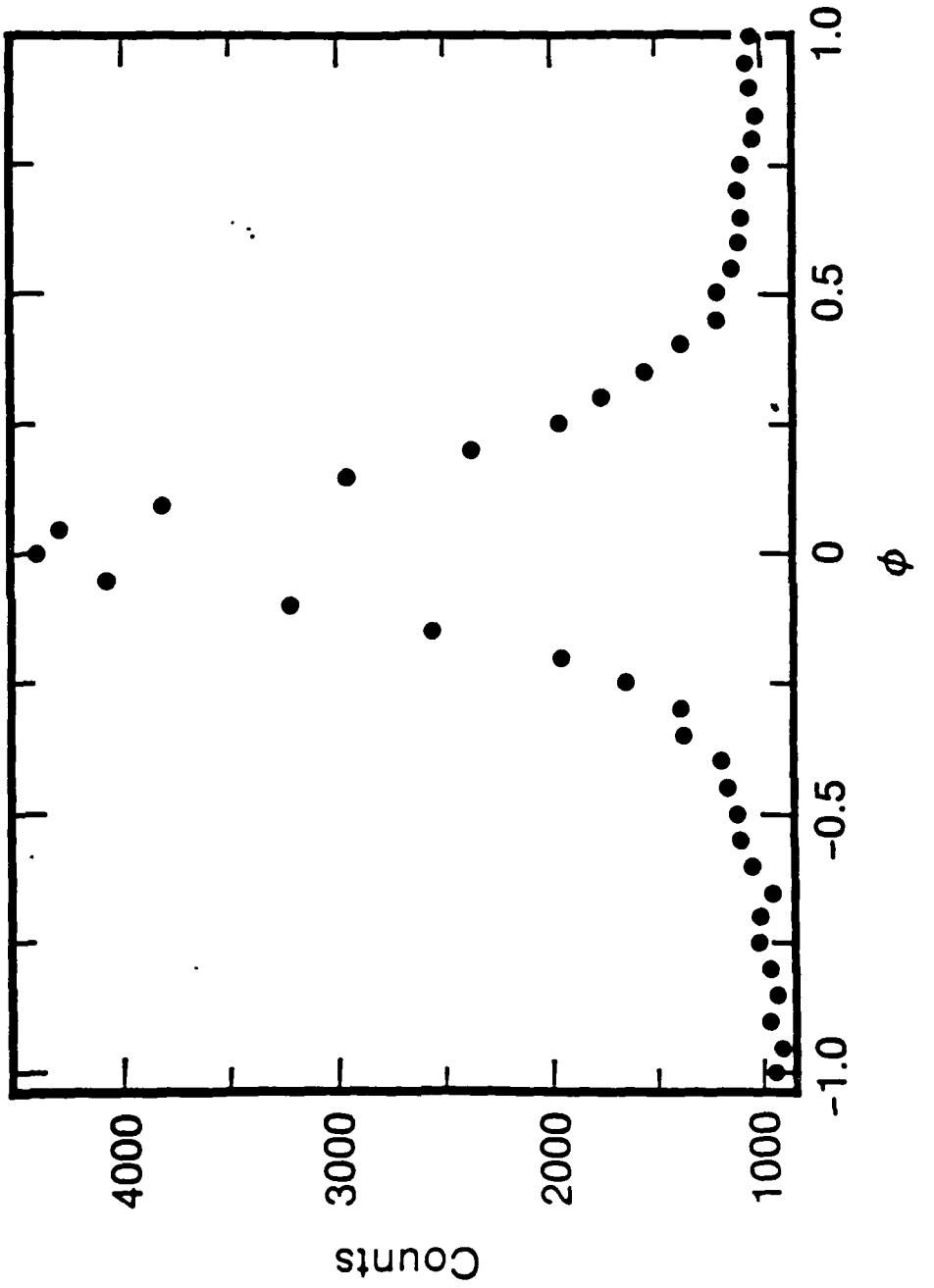

Fig 3 b

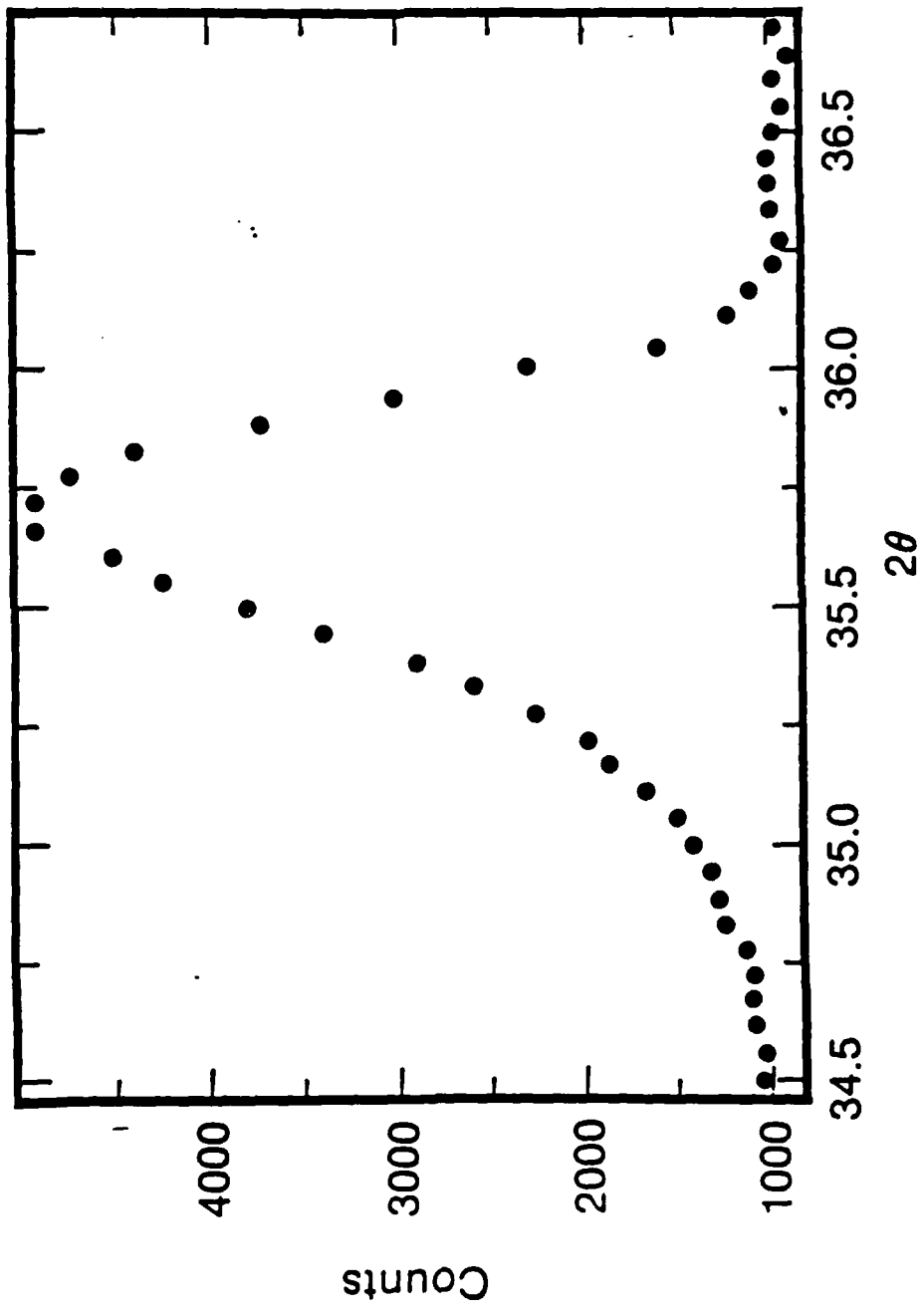

Fig 3c

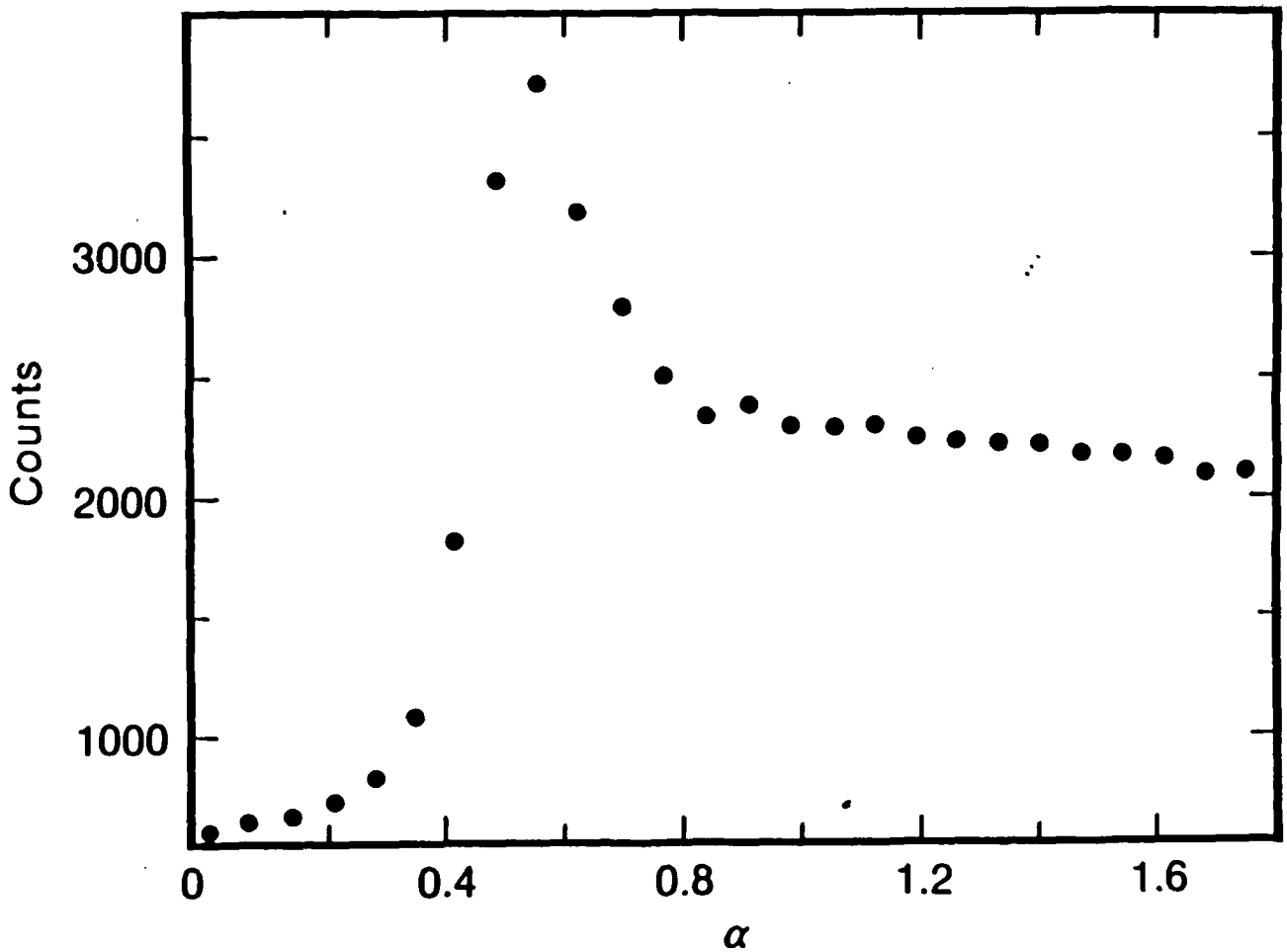

Fig 4c

Fig 45

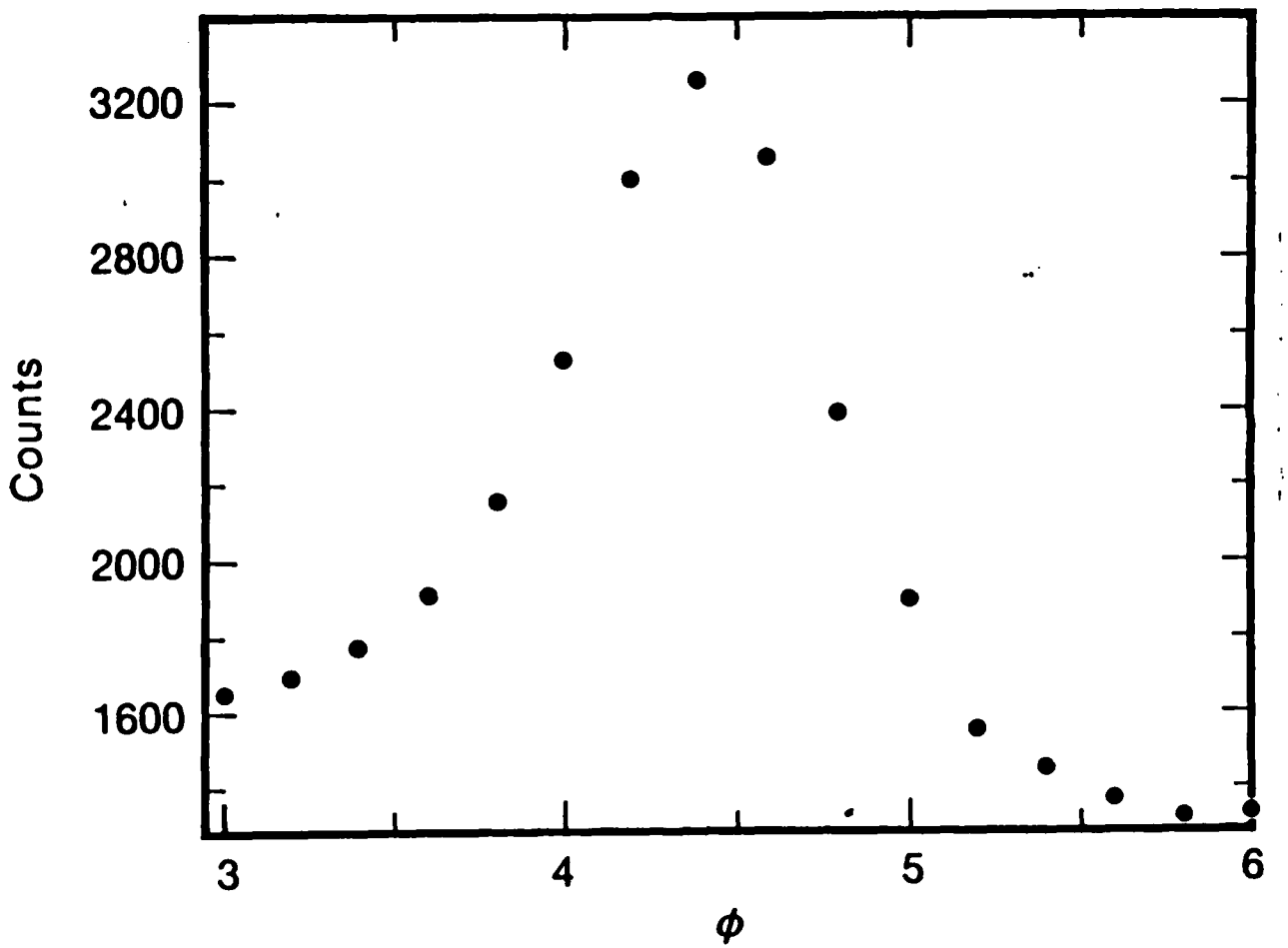

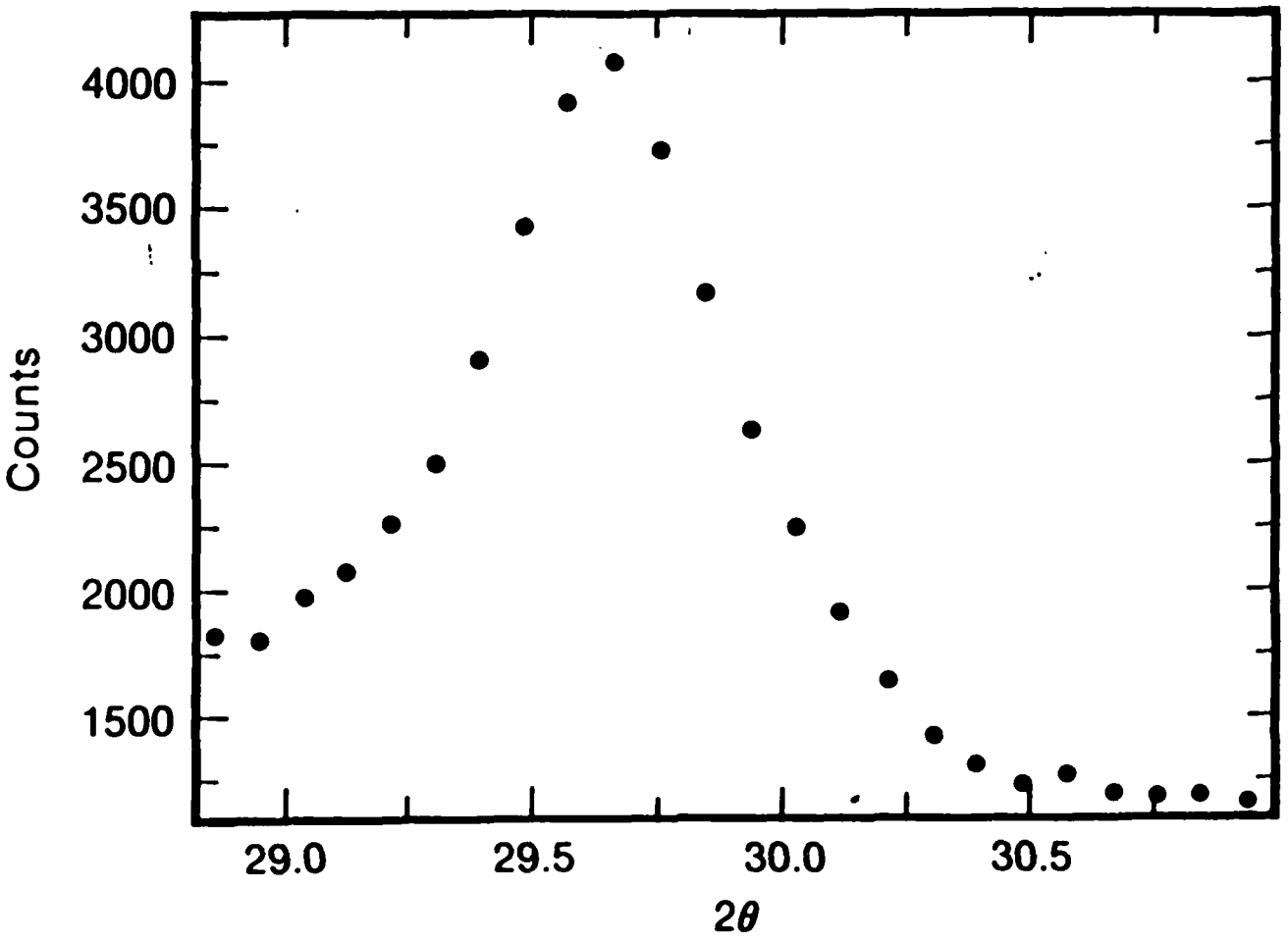
4000
3500
3000
2500
2000
1500
Counts
29.0
29.5
30.0
30.5
2θ

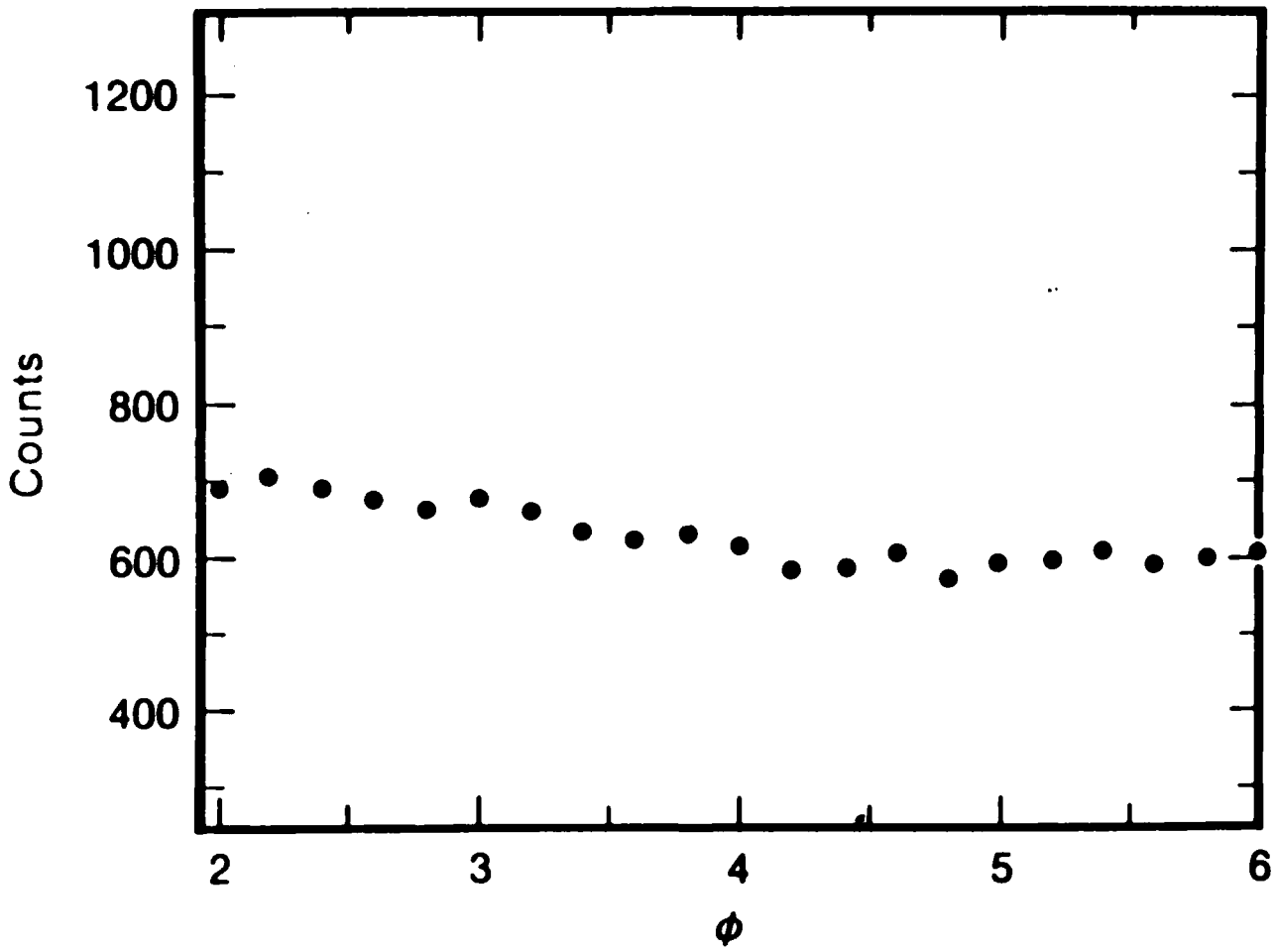
1200
1000
800
600
400
Counts
2
3
4
5
6
φ

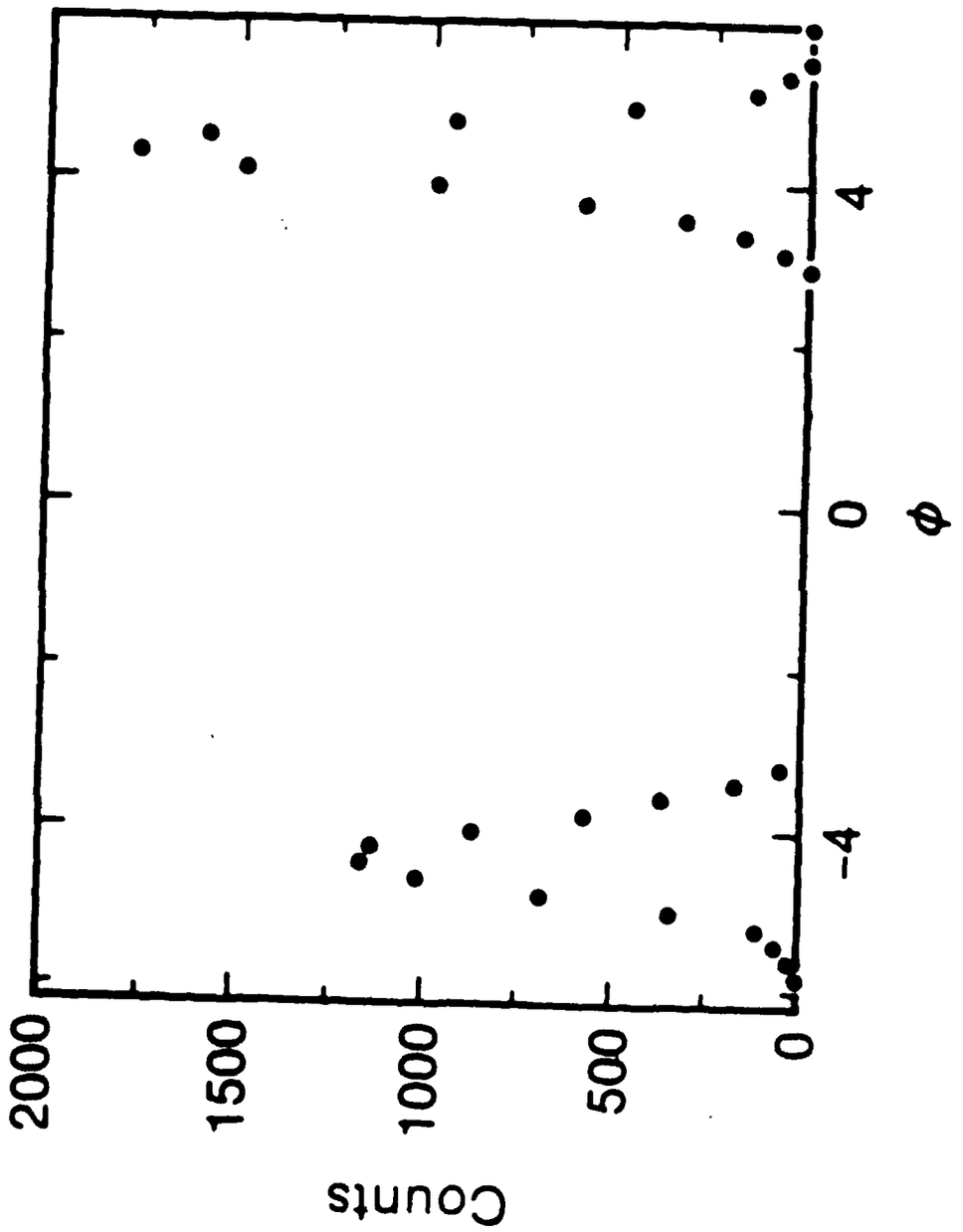

Fig 6c

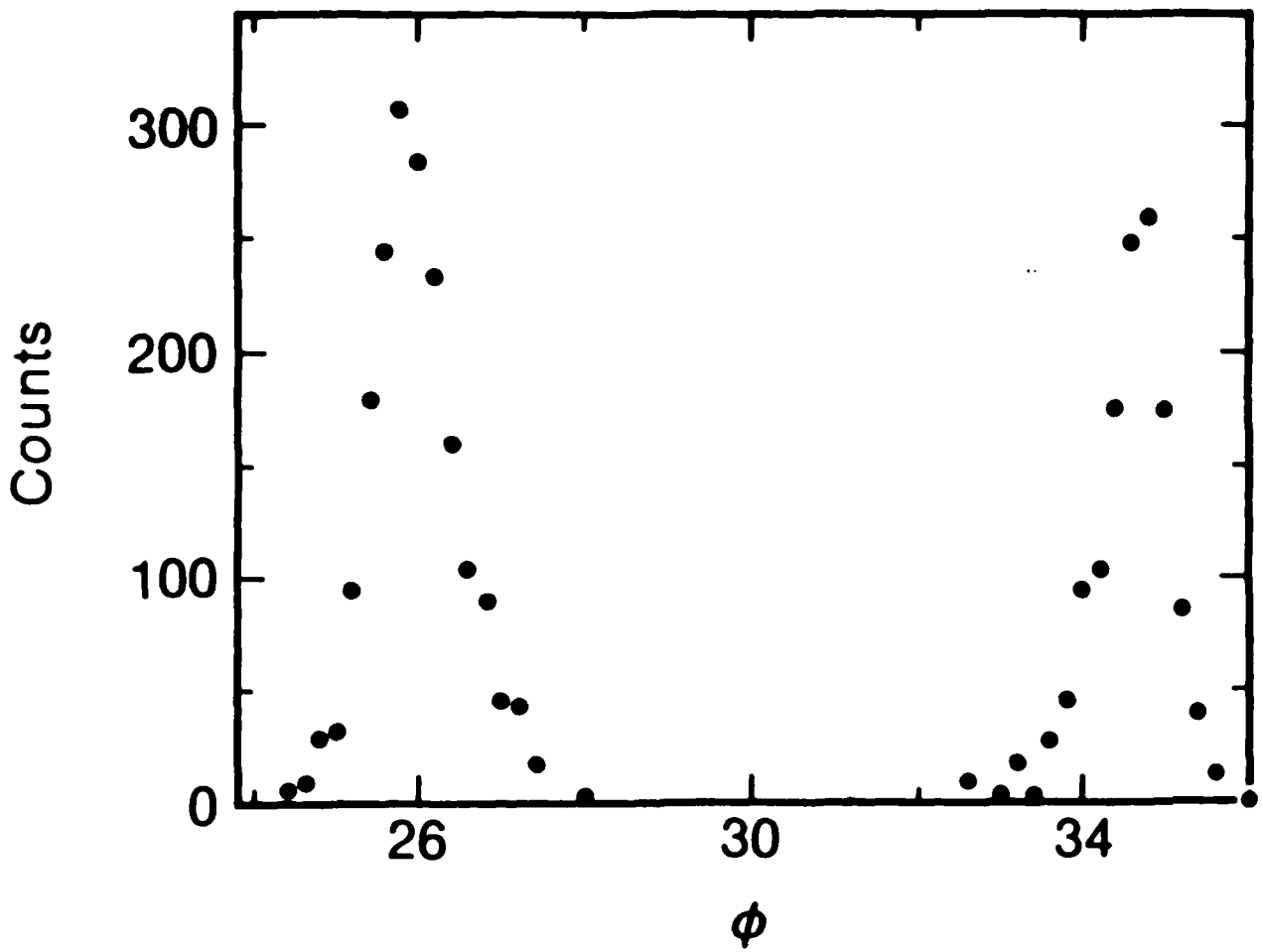
300
200
100
0
Counts
26
30
34
ϕ

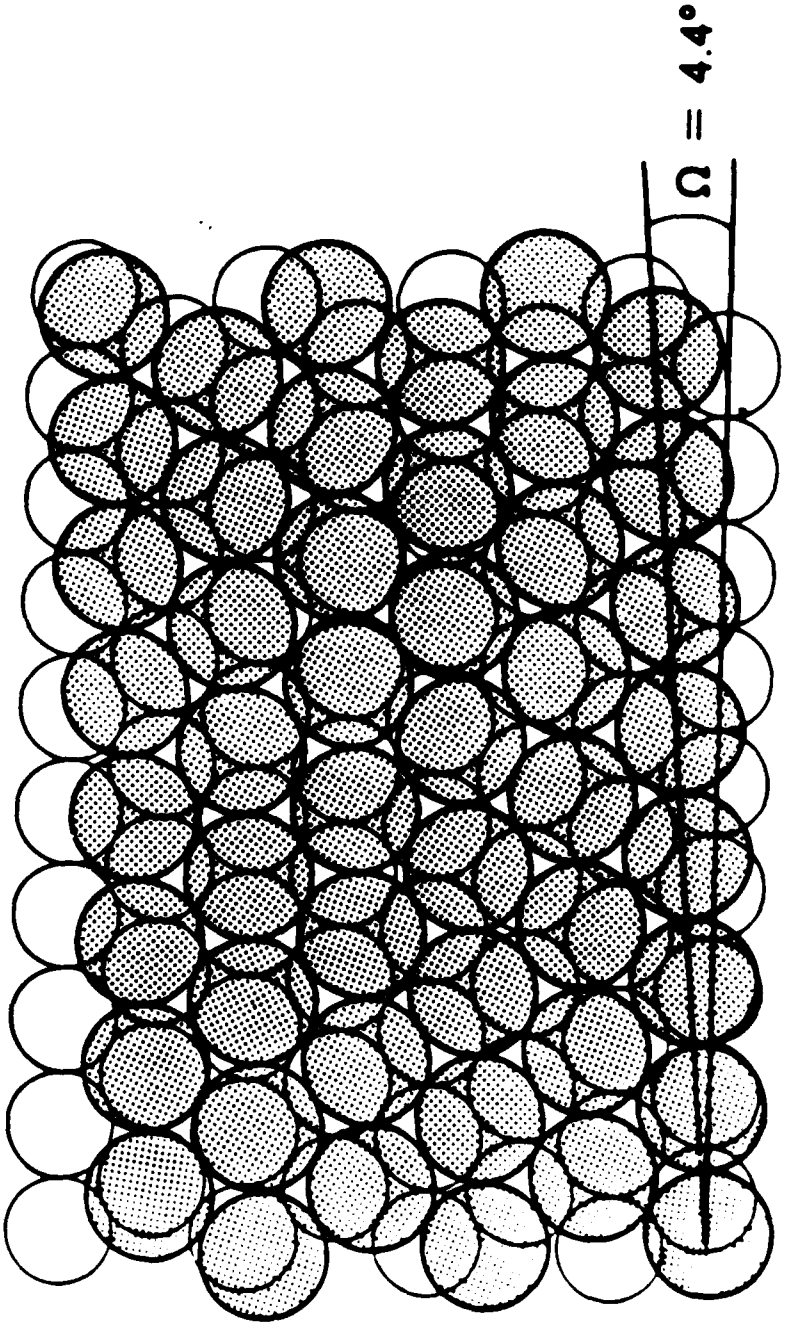

Fig 7a

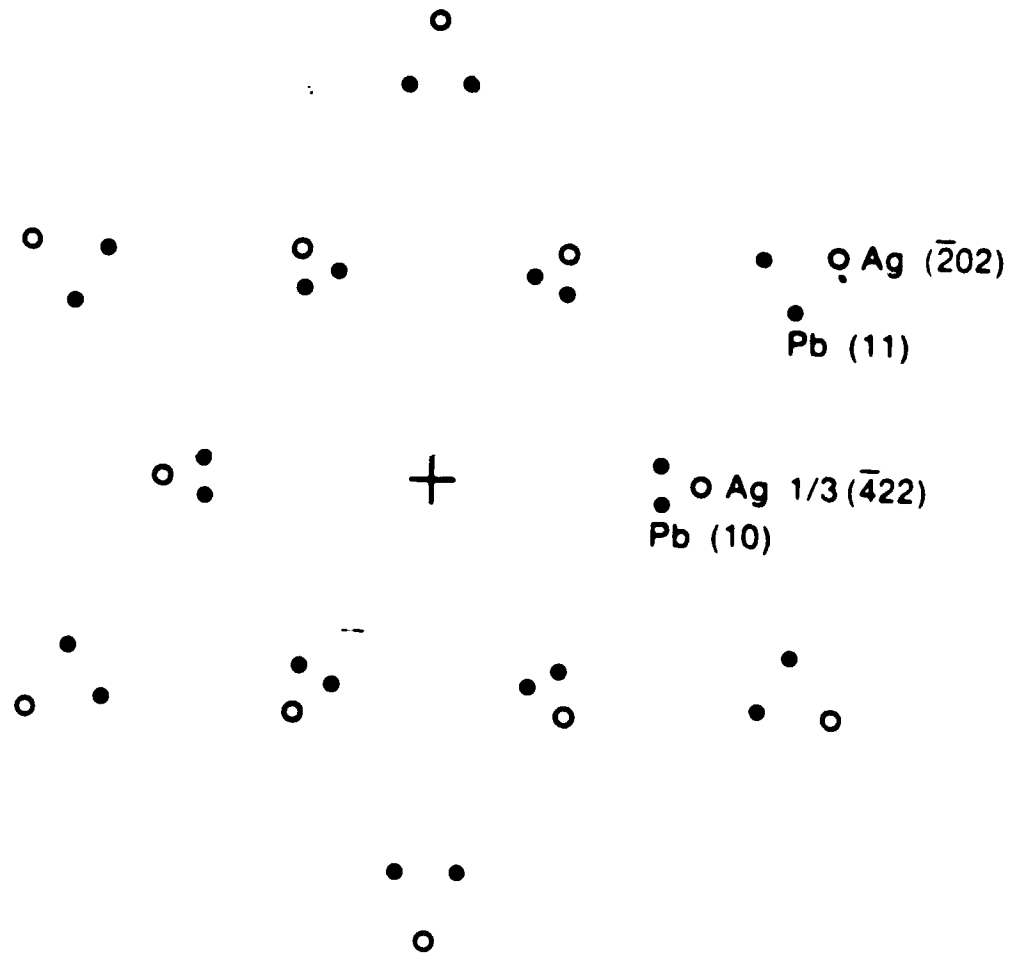

Fig 7b

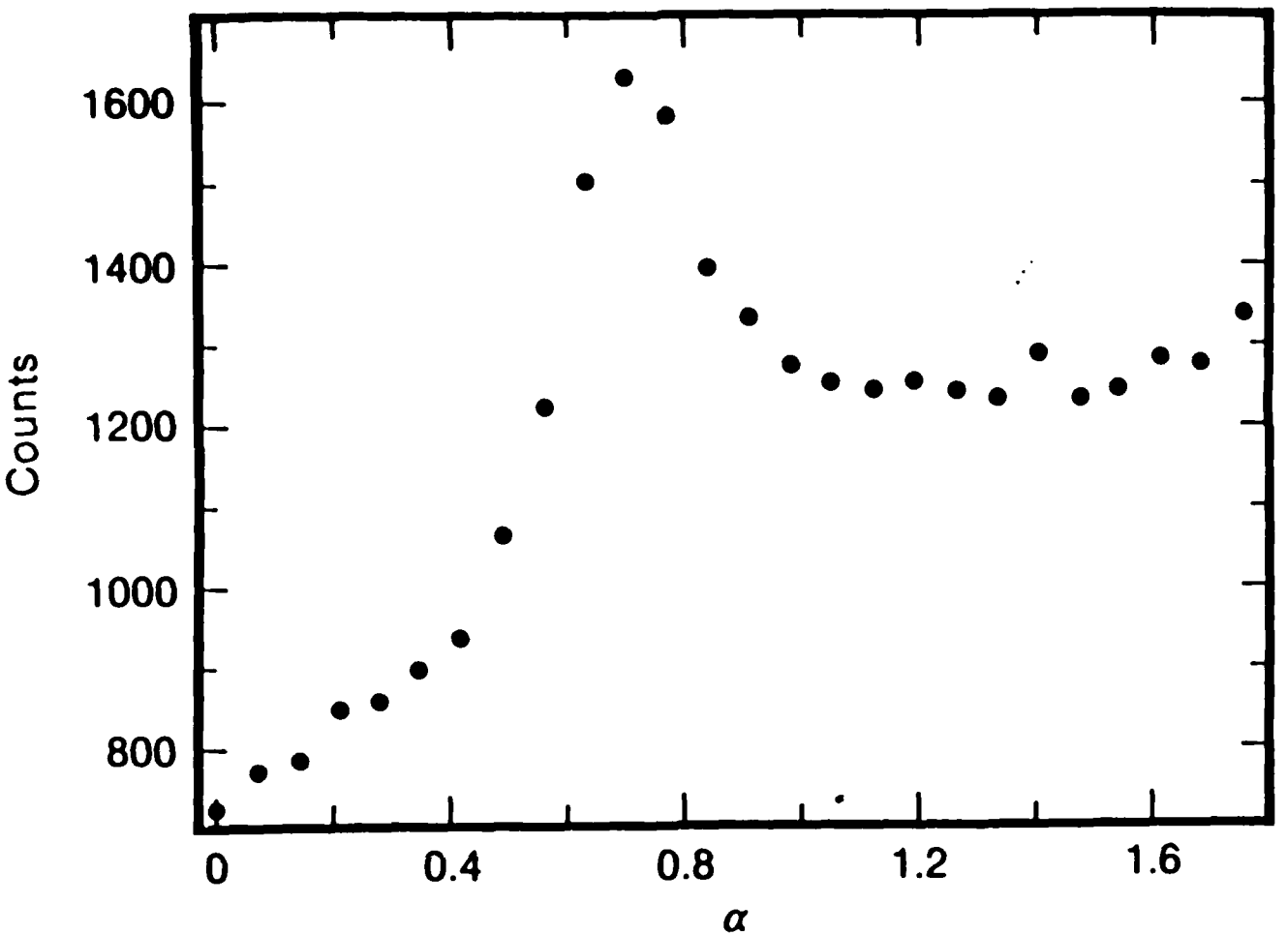

Fig 8

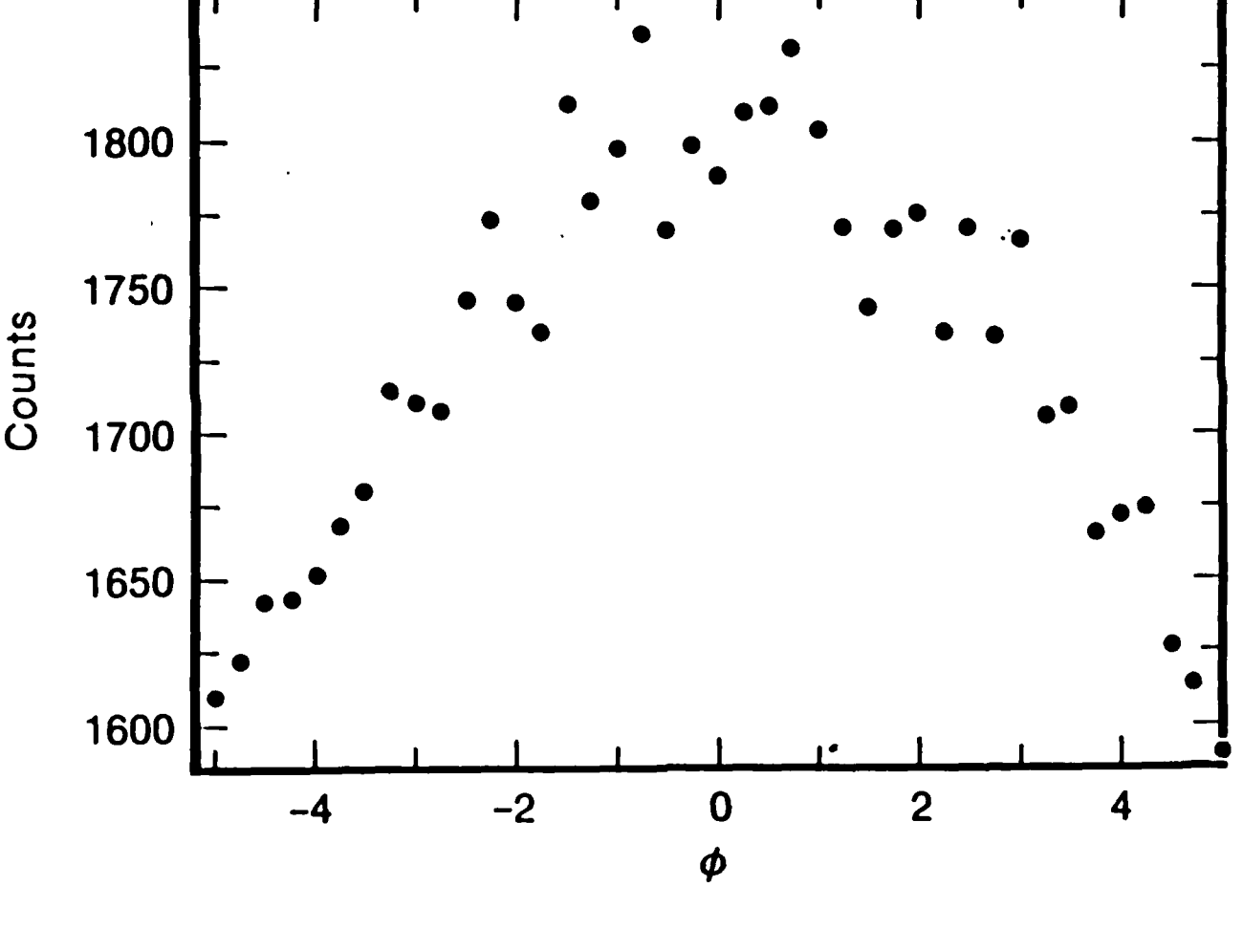

Fig 85

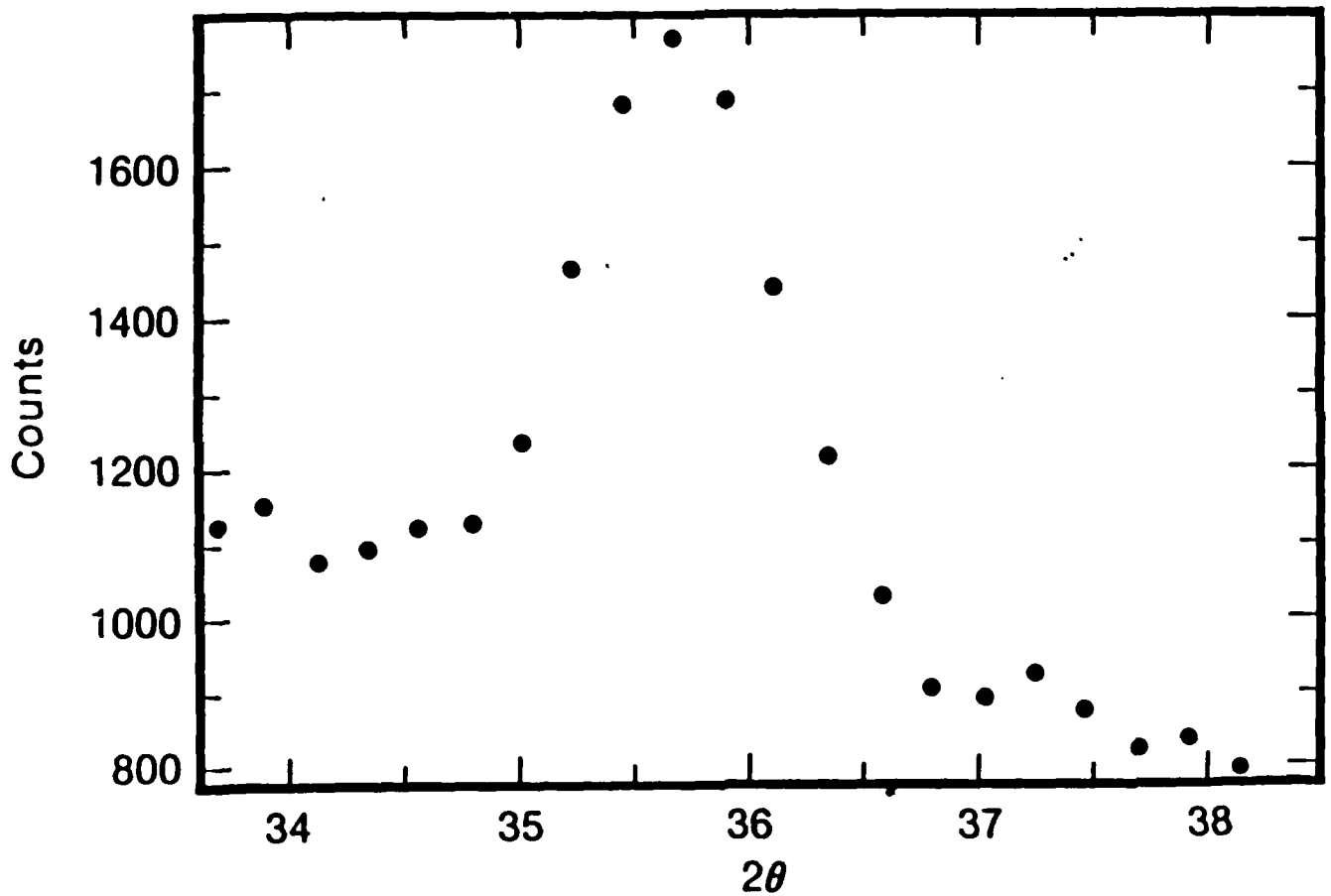

Fig 8.

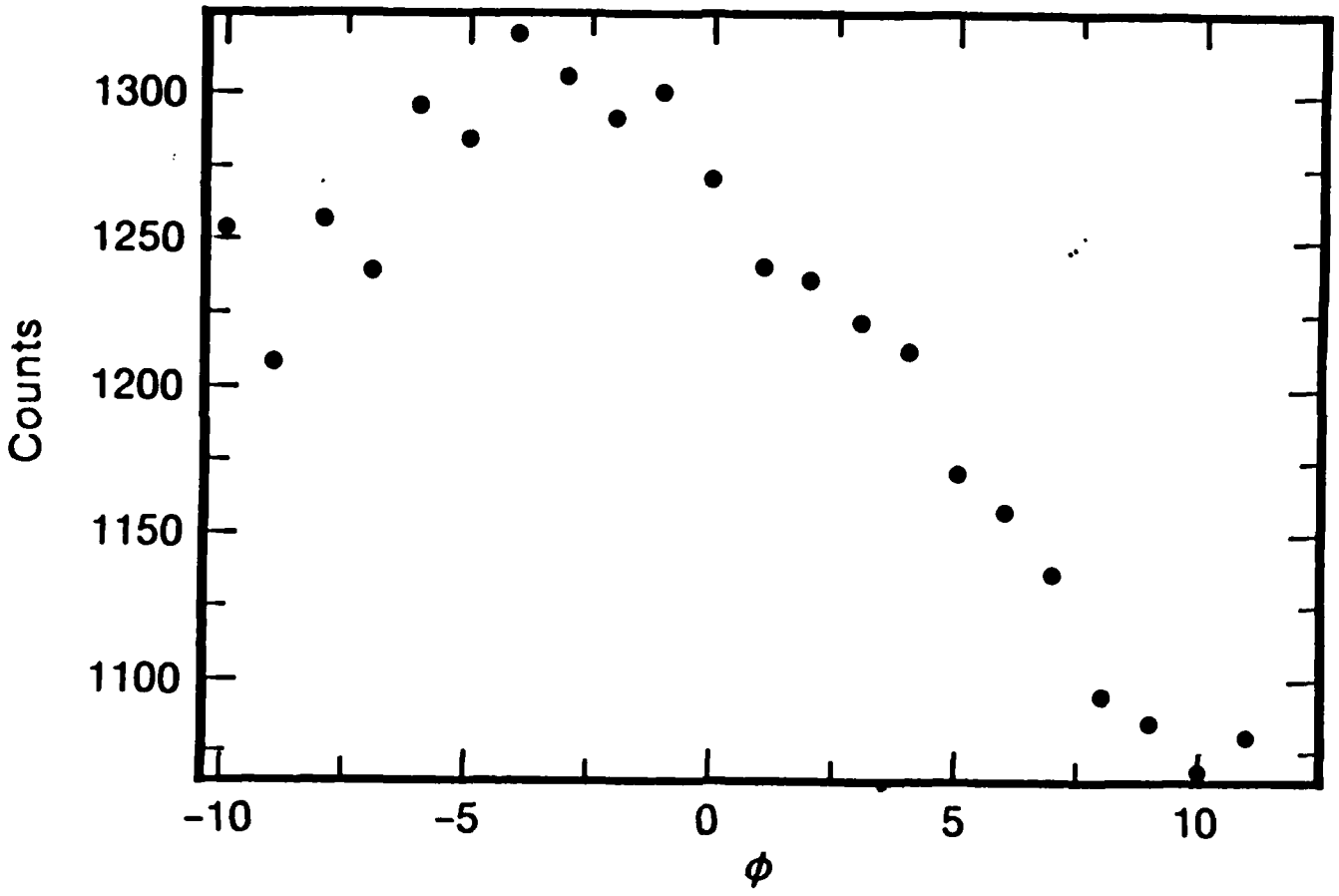
1300
1250
1200
1150
1100
Counts
-10
-5
0
5
10
φ

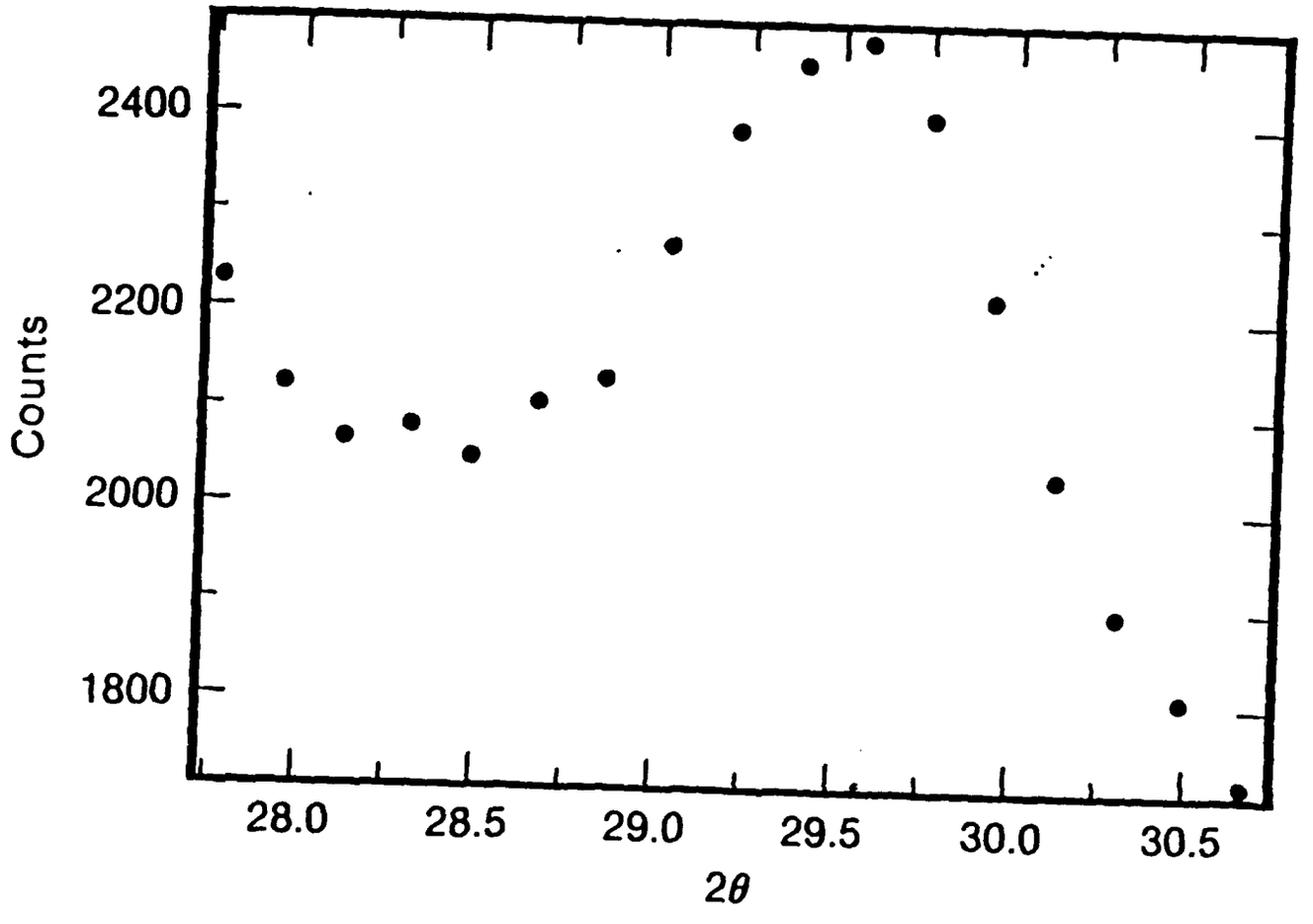
2400
2200
2000
1800
Counts
28.0
28.5
29.0
29.5
30.0
30.5
2θ

END

7-87

DTIC